










Letter

Quantitative comparison of impurity transport in turbulence reduced and enhanced scenarios at Wendelstein 7-X

J.A. Alcusón^{1,2,a,*} , Th. Wegner^{1,a} , A. Dinklage¹ , A. Langenberg¹ , J.-P. Böhner³ ,
B. Buttenschön¹ , E.M. Edlund⁴, G. Fuchert¹, J.M. García-Regaña⁵ , O. Grulke^{1,6},
Z. Huang⁷, M. Porkolab³, A.V. Stechow¹, P. Xanthopoulos¹ , A. Zocco¹ 
and the W7-X Team^{1,b}

¹ Max-Planck Institute for Plasma Physics, 17491 Greifswald, Germany

² Laboratorio de Innovación en Plasmas, University of Cordoba, 14071 Córdoba, Spain

³ MIT Plasma Science and Fusion Center, Cambridge, MA 02139, United States of America

⁴ SUNY Cortland, Cortland, NY 13045, United States of America

⁵ Laboratorio Nacional de Fusión, CIEMAT, Av. Complutense, Madrid 28040, Spain

⁶ Technical University of Denmark, 2800 Kongens Lyngby, Denmark

⁷ UKAEA, Culham Centre for Fusion Energy, Culham Science Centre, Abingdon, Oxon OX14 3DB, United Kingdom of Great Britain and Northern Ireland

E-mail: jorge.alcuson@ipp.mpg.de

Received 21 April 2023, revised 2 July 2023

Accepted for publication 28 July 2023

Published 9 August 2023



CrossMark

Abstract

We assess the turbulent particle transport being responsible for the limitation of the confinement and, thus, the overall performance of the neoclassically optimized stellarator Wendelstein 7-X. The radial particle transport is experimentally inferred from the evaluation of impurity injection into turbulence reduced and enhanced plasma scenarios revealing a completely different confinement behavior. The impact of the density gradient on the turbulent ion transport is theoretically estimated using large-scale non-linear gyro-kinetic simulations enabling, for the first time in Wendelstein 7-X, a quantitative comparison to the experimentally assessed impurity transport properties. We demonstrate that impurity transport in most of the Wendelstein 7-X discharges, up to now impossible to cover only with neoclassical estimations, is dominated by turbulence and can be modelled via gyro-kinetic simulations.

^a These two authors contributed equally.

^b See Sunn Pedersen *et al* 2022 (<https://doi.org/10.1088/1741-4326/ac2cf5>) for the W7-X Team.

* Author to whom any correspondence should be addressed.



Original Content from this work may be used under the terms of the [Creative Commons Attribution 4.0 licence](https://creativecommons.org/licenses/by/4.0/). Any further distribution of this work must maintain attribution to the author(s) and the title of the work, journal citation and DOI.

Keywords: turbulent transport, impurity transport, stellarator, plasma

(Some figures may appear in colour only in the online journal)

1. Introduction

Stellarators embody one concept for the production of magnetically confined fusion energy. As stellarators enable a steady state plasma operation, the control and improvement of the performance of those fusion devices is one of the most important topics in fusion research. The performance is, amongst others, limited by confinement properties of particles, heat and momentum being set by collisional (classical and neoclassical) and anomalous transport which is often attributed to turbulence. At the same time, impurity sources are unavoidable in fusion devices because the first wall erosion during discharges liberates impurities in the plasma. If these expected but not invited species persist inside the plasma and accumulate in the core, they can lead to a radiative collapse degrading the performance of the machine. In general, heavy impurity species tend to accumulate in the plasma core due to the action of the neoclassical transport in fusion devices [1–4]. This problem is significantly relevant for stellarators, with a high neoclassical contribution compared to tokamaks. Nevertheless, Wendelstein 7-X fusion device (W7-X) is the first optimized stellarator to reduce the neoclassical transport down to tokamak levels [5]. And, for that reason, the absence of impurity accumulation in most of the W7-X discharges [6] has immediately pointed to the turbulent component of the transport to flush these species out of the machine [7–9], highlighting the relevance of a dedicated study for the impurity turbulent transport in such device.

Turbulence mechanisms at ion-scale are caused by low-frequency plasma micro-instabilities such as the ion-temperature gradient (ITG) driven mode and the trapped electron mode (TEM). Particularly for W7-X at low density gradients, the turbulence level of TEM is rather benign due to the magnetic field geometry [10, 11]. Thus, the ITG mode [12–14] is expected to be the dominant turbulence mechanism which is driven by the normalized ion temperature gradient length, $a/L_{T_i} = -(a/T_i)dT_i/dr$, ($a = 0.52$ m is the minor radius of the torus and r the effective plasma radius) and stabilized by the normalized electron density gradient length, $a/L_{n_e} = -(a/n_e)dn_e/dr$. In plasma scenarios with peaked density profiles where $a/L_{T_i} \sim a/L_{n_e}$, the ITG in W7-X is reduced leading to less transport and enhanced confinement [15–17]. In standard electron cyclotron heated (ECRH) plasmas with gas fueling, the density gradient in W7-X is usually low and thus the ITG mode is dominant, limiting the confinement of particles and heat. Main aspects of the resulting turbulent transport has recently been discussed in experimental [7–9] and theoretical [8, 16–21] work, however, the direct comparison between the results is still lacking for impurity turbulent transport in W7-X. Some publications have indirectly pointed out the necessity of a strong contribution of turbulence to the impurity transport in ECR heated plasmas

(dominant ECR heating without kinetic profile shaping events, e.g. pellet injection) to explain the enormous discrepancies between the neoclassical estimations and total transport in some discharges [7], the impurity transport independence on the charge state [9, 19] and the impact of temperature ratio [8] on impurity transport. Our results demonstrate that a gyro-kinetic modelling of turbulence could explain all these phenomena reproducing the transport coefficients for a specific discharge at the same time. In particular, this manuscript quantitatively compares the experimentally and theoretically inferred ion-scale turbulent particle transport in the core of W7-X for *reduced* (turb \downarrow) and *enhanced* (turb \uparrow) *turbulence plasma scenarios*. Large-scale non-linear gyro-kinetic simulations have been successfully performed, which reflect very well the experimental results obtained from transport investigations by means of non-intrinsic impurity injection. These findings motivate the further application of gyro-kinetic simulations for comprehensive turbulence studies and might be a key tool for the development of turbulence optimized fusion reactors.

2. Experimental analysis

2.1. Experimental setup

Two experimental programs from the previous OP1.2b operation campaign of W7-X with uncooled carbon divertor were selected. They were executed in the standard magnetic field configuration [22] with hydrogen as main fuel gas and exhibit low-beta, i.e. a low plasma to magnetic pressure ratio. The programs are excellent candidates for comparison because they have very similar plasma parameters except for the density gradient and thus reflect the turbulence reduced and enhanced scenario. In particular, the on-axis ECRH power deposition (within $0 \leq r/a \leq 0.15$) as well as the electron density and temperature and the ion temperature are comparable for both programs, see figures 1(a) and (b). In each scenario, similar trace amounts (less than 10^{17} atoms and $n_{\text{Fe}}/n_e < 10^{-5}$) of iron were injected by means of a laser blow-off (LBO) system [23, 24]. The injected iron particles are ionized and excited in the plasma and start to emit line emission. Figure 1(c) exemplary illustrates the spectroscopic measurement of the Fe XXV line emission in the x-ray spectral range [25, 26] for both programs. It is obvious, that the temporal behavior of the line emission is completely different. In the turbulence enhanced scenario, a clear decay of the Fe XXV is observable and provides an impurity transport time of 130 ± 5 ms, being a measure for the impurity confinement of trace ions in the plasma [23]. In the turbulence reduced scenario, the Fe XXV line emission increases until the discharge is distorted by pellet injections (0.5 s after the injection) leading to different densities, temperatures and in the end to different excitation rates

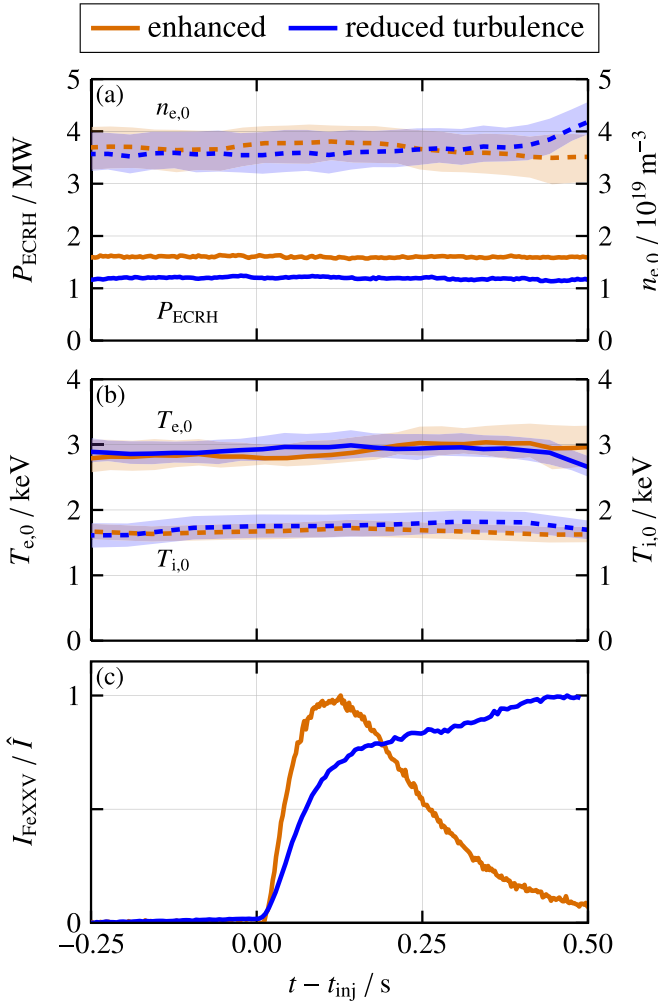


Figure 1. Time traces of the ECRH power and center electron density (a), center electron and ion temperature (b) and the normalized Fe XXV line emission (c) for the reduced (blue, 20 180 919.007) and enhanced (orange, 20 180 919.049) turbulence scenario.

and a drop of the Fe XXV emission. This case might be an indication of accumulation although this is not verifiable due to the preliminary termination of the discharge. Although the impurity injection provides intense spectral emission lines of different iron ionization stages, the global plasma parameters are barely changed, see also figure 1. This is a crucial condition for the spectroscopic evaluation and the below described estimation of the transport properties. It should be additionally mentioned that for the turbulence reduced scenario a neutral beam injection (NBI) heated period ends 500 ms before the impurity injection. After the NBI phase, ECRH is applied exclusively.

Figure 2 shows profile fits of the experimental data for the electron density, n_e , the ion, T_i , and electron, T_e , temperature, respectively. They are determined at times where the main plasma parameters are virtually constant and where an effect of the impurity injection can be ruled out. The fitted curves result from a Gaussian process fit to the data that are mapped to the effective radius, r/a , employing a magnetic equilibrium

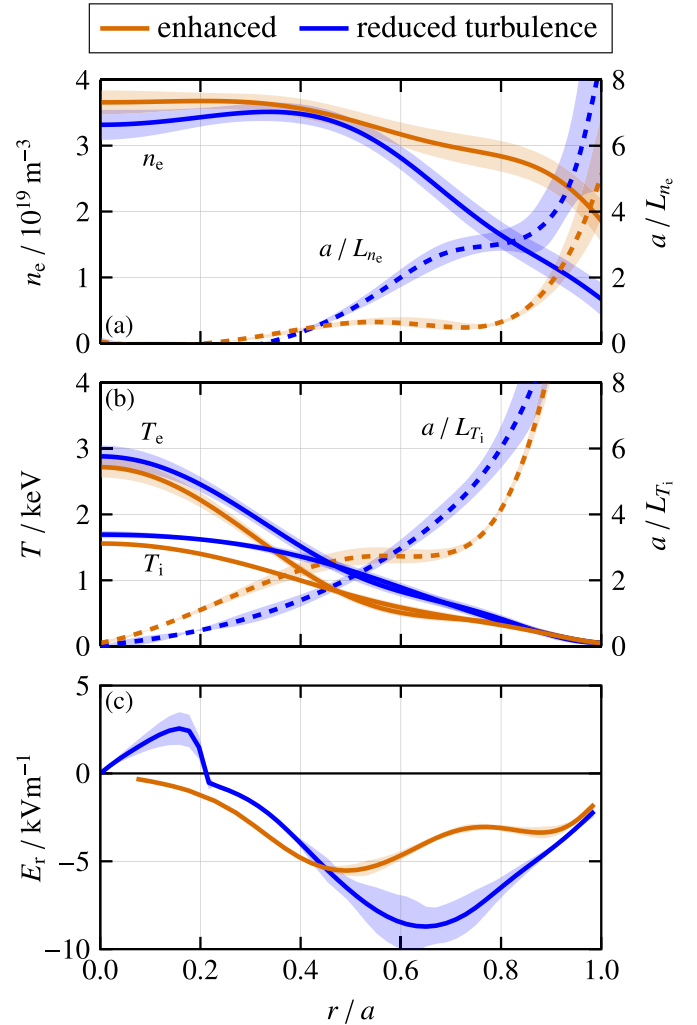


Figure 2. Fits (solid lines) and normalized gradient length (dashed lines) of the electron density (a), ion and electron temperature (b) and ambipolar electric field generated with DKES (c) profiles as a function of the plasma radius for the reduced (blue, 20 180 919.007) and enhanced (orange, 20 180 919.049) turbulence scenario.

calculation by means of the variational moments equilibrium code (VMec) [27]. Profiles are provided with an estimation for the fitting error, see the shaded area in figure 2. These uncertainties will be employed in further analysis, allowing us to assess the robustness of the findings in terms of this small deviations. The fits take into account Thomson scattering data (n_e , T_e) [28] and measurements from the x-ray imaging spectroscopy (T_i) [26]. The ion temperature is set to the electron temperature for $T_i > T_e$ since excess energy flow from the electrons to the ions can be excluded in the purely electron heated plasma. Moreover, bolometer measurements do not indicate any excess energy sink for the radiation. From these fits, the normalized ion temperature gradient as well as the normalized electron density gradient are inferred serving as input for the non-linear gyro-kinetic simulations. The center density of both discharges are similar albeit the gradient in the outer core are different resulting into a higher normalized density gradient for the turbulence reduced scenario. The profiles of

the temperatures and therewith the normalized gradients are comparable for both cases. Calculating the ambipolar electric field with the drift kinetic equation solver (DKES) [29] results in values of about -10 kVm^{-1} (turbulence reduced scenario) and -5 kVm^{-1} (turbulence enhanced scenario) as the maximum strength in the outer half of the plasma volume, see figure 2(c). Except for the very core, the ambipolar field becomes negative for both scenarios indicating a neoclassical ion root feature [30]. The neoclassical energy flux is way smaller than the applied heating and goes up to about 30% for the turbulence reduced but no more than 18% for the turbulence enhanced scenario.

2.2. Transport analysis with STRAHL

The experimental approach to infer transport properties includes the application of the spectroscopic measurement of injected impurities in the ultraviolet [31] and x-ray spectral range [25, 26]. In particular, the temporal evolution of the emission from various charge states of iron is calculated forward with the one-dimensional impurity transport code STRAHL [32] and is being compared with measured data. Using an iterative optimization procedure [7], the radial diffusion profile, D , is inferred to match the local impurity flux $\Gamma = -D\nabla n + vn$ for the impurity density, n , and hence to adapt the measured emission time traces. The convection velocity, v , profile is assumed to be the sum of classical and neoclassical parts being derived from DKES and amounts to about 0.3 ms^{-1} (line-averaged). For the turbulence enhanced scenario, thermo-diffusion is additionally accounted for by normalizing the temperature gradient profile to the absolute value of the thermo-diffusion pinch calculated from turbulent modeling at the radial position argued in section 3. This gives an additional contribution to the convection of about -0.75 ms^{-1} (line-averaged). For the comparison between the inferred and neoclassical diffusion profiles, the neoclassical diffusion coefficients are additionally determined with DKES and shown in figure 5. It is known that the collision operator of DKES becomes less accurate at higher collisionalities (here highly ionized Fe atoms). However, a comparison with neoclassical calculations from SFINCS [33], which do not show this inaccuracy, has shown that the deviation is negligible even for higher collisionalities. Also, considering such an insignificant contribution to the total transport [7], this model should be enough. As reported before in the literature [7], the neoclassical diffusion coefficient is on the order of $0.001\text{ m}^2\text{ s}^{-1}$. This is a factor of 100 smaller compared to the profile averaged values of the inferred turbulent diffusion coefficients for dominant ECR heated plasmas without kinetic profile shaping events. Beside to the above mentioned kinetic profiles, STRAHL is supplied with the neutral background density since it affects the charge stage distribution via charge-exchange collisions. The neutral density is calculated with the KN1D code [34] that requires, among others, the neutral density close to the wall [7]. Unfortunately, this information is not available and therefore the neutral background density is scaled-up with a factor f_{H^0} so that the pressure and recombination limits are not exceeded. In addition

to that, the mach number M and therewith the parallel flow velocity is an important input parameter for STRAHL since it describes the parallel loss time into the divertor at a known connection length. STRAHL is also supplied with the timing of the impurity injection t_{LBO} since this information is important for the matching of lower ionization stages and in the end for the determination of the diffusion coefficient in the edge. Unfortunately, the three parameters f_{H^0} , M and t_{LBO} are unclear and therefore are varied in a reasonable range and permuted for each iterative optimization procedure. As a result of that, about 4×10^4 radial diffusion profiles are inferred for each scenario. These can be weighted by the goodness of the fit convoluted with the amount of similar profiles. Hence, the most likely fit result as well as areas with lower probability can be determined with that method and are visualized in figure 5 as solid lines and shaded areas, respectively.

3. Turbulent modelling

The turbulent flux along the radial direction for impurity tracer concentrations is described by three contributions: a diffusive term $\Gamma_D^{(Z)}$, a thermo-diffusive term $\Gamma_\chi^{(Z)}$ and a curvature pinch $\Gamma_C^{(Z)}$,

$$\Gamma_{\text{total}}^{(Z)} = \Gamma_D^{(Z)} + \Gamma_\chi^{(Z)} + \Gamma_C^{(Z)} = -D_Z \nabla n_Z + \chi_Z \nabla T_Z + C_Z n_Z \quad (1)$$

where the diffusion D_Z and thermo-diffusion χ_Z coefficients only depend on the background turbulence of the main ion species, and the curvature pinch C_Z is a geometrical pinch [18]. These transport coefficients are independent of the impurity gradients, temperature and density, because of the trace concentration approximation. In other words, the background turbulence produced by ions and electrons is not modified by the presence of impurities due to their insignificant concentration. Gyro-kinetic simulations are computationally very demanding, thus, we will take advantage of some previous results to simplify our modelling. In particular at W7-X, the thermo-diffusion and the curvature pinch in equation (1) have a low contribution compared with the diffusive term and become relevant to the total flux only for very reduced density gradients [19]. This is particularly relevant for the thermodiffusion coef. of heavy impurities like iron where $\chi_Z \propto 1/Z^2$ [18]. Considering our two experimental scenarios, these terms will affect our results for the enhanced turbulence plasma, where the density gradient is low, and will not be considered for the reduced turbulence scenario due to a significant $a/L_{n_{\text{Fe}}}$. For simplicity, due to the independence of the transport coefficient on the impurity density gradient, we will use same density and temperature gradient for main ions and impurities ($a/L_{n_{\text{Fe}}} = a/L_{n_i}$, $a/L_{T_{\text{Fe}}} = a/L_{T_i}$) in both scenarios without lack of generality for our results. In that sense, in the enhanced turbulence scenario modelling we will perform two identical simulations: one with the $a/L_{n_{\text{Fe}}} = a/L_{n_i}$ and $a/L_{T_{\text{Fe}}} = a/L_{T_i}$ to estimate the total particle flux Γ_{tot} including $T_i = 0.5\text{ keV}$, $a/L_{T_i} = 2.8$, $a/L_{n_e} = 0.6$, and another one with $a/L_{n_{\text{Fe}}} = 0$ to estimate the contribution of the thermo-diffusion and the curvature pinch

isolated in one pinch term $\Gamma_V^{(Z)} = \Gamma_X^{(Z)} + \Gamma_C^{(Z)}$. This pinch will be included in STRAHL calculations, see section 2.2, to have a consistent estimation of the coefficient D_Z with both codes. From the difference between both terms, we can estimate the diffusive contribution $\Gamma_D^{(Z)} = \Gamma_{\text{total}}^{(Z)} - \Gamma_V^{(Z)}$. For the reduced turbulence scenario, only one simulation with all the gradients included $a/L_{T_i} = 3.0$, $a/L_{n_e} = 2.1$ and $T_i = 0.75$ keV is performed to estimate the total flux.

The gyro-kinetic simulations are performed with an Eulerian solver, the GENE code [35]. Our model, previously used to investigate stellarator turbulence [36] including the W7-X geometry [17, 24], considers a flux-tube scheme, three kinetic species (main ions H^+ , electrons e^- and iron impurities Fe^{25+}), electrostatic fluctuations, and no collisions. Non-linear simulations have a domain $(L_x, L_y, L_z) = (125, 125, 2\pi)$ and a resolution of $(n_x, n_y, n_z, n_{v_{||}}, n_\mu) = (128, 128, 128, 32, 9)$. The standard magnetic field configuration [22] is considered as magnetic geometry. The impurity-electron density ratio with $n_{Fe}/n_e = 10^{-8}$ guarantees the trace concentration of iron in the simulations. In W7-X, ITG-turbulence is radially localized in a region around $0.5 < r/a < 0.7$ [37, 38]. Our simulations are performed at $r/a = 0.6$, where the ‘anomalous’ contribution estimated by STRAHL was found maximum in previous works [7]. The above mentioned parameters used for the calculations are the experimental values at this radial position. In the outer half of the plasma as illustrated in figure 2, main species are strongly coupled and share same temperature $T_e/T_i = 1$. Since the electron temperature gradient (ETG) instability in W7-X does not play an important role for transport compared with ITG and TEM instabilities [39], we will consider no electron temperature gradient $a/L_{T_e} = 0$ as it is usual in numerous W7-X studies [17, 24].

3.1. Linear simulations

Firstly, a linear study of the different instabilities is provided. Linear growth rates γ for both scenarios are illustrated in figure 3. The growth rate spectrum for the enhanced turbulence scenario shows an important and dominant ITG instability at ion scales, around $k_y \rho \approx 0.9$, and a typical broad TEM plateau for intermediate scales. Using a quasi-linear transport model, where $D_i \propto \gamma/k_y^2$, we can argue that the dominant instability for ions should be ITG. In the turbulence reduced scenario, the ITG linear growth rate is reduced and almost located at the same scale ($k_y \rho \approx 1$). In contrast, the linear growth rate associated to the TEM instability is increased in this scenario and closer to ion scales (almost fused with the ITG instability, peaking at $k_y \rho \approx 1.6$). In this scenario, a quasi-linear argument suggests again an ITG-dominant instability for ions, but the difference between the transport coefficients is, in this case, reduced due to a similar growth rate and mode scale.

3.2. Non-linear results

The heat Q_i and particle Γ_i fluxes of the different scenarios are shown for main ions in figure 4. We observe an important difference of heat flux between the two scenarios. The reduction of the heat flux is produced by the density peaking of the

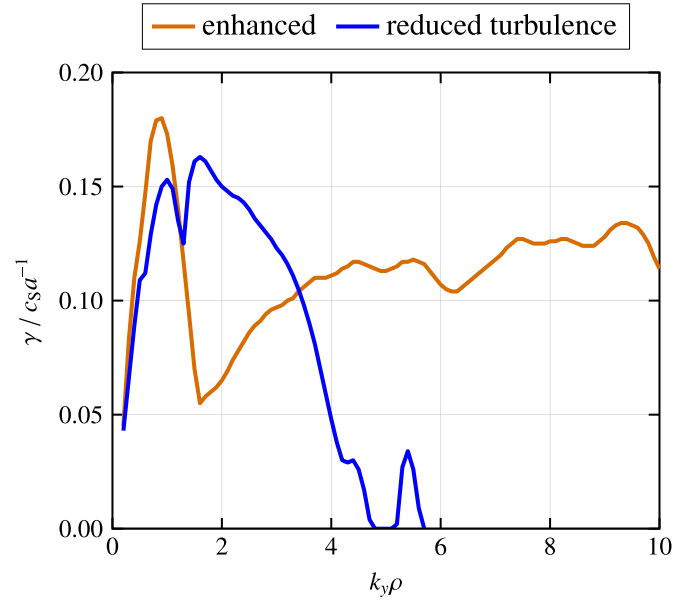


Figure 3. Linear growth rate wavenumber spectrum generated with GENE for the reduced (blue, 20 180 919.007) and enhanced (orange, 20 180 919.049) turbulence scenarios. Units: $c_s = \sqrt{2T_i/m_i}$ is the ion sound speed inside the plasma and a the minor radius.

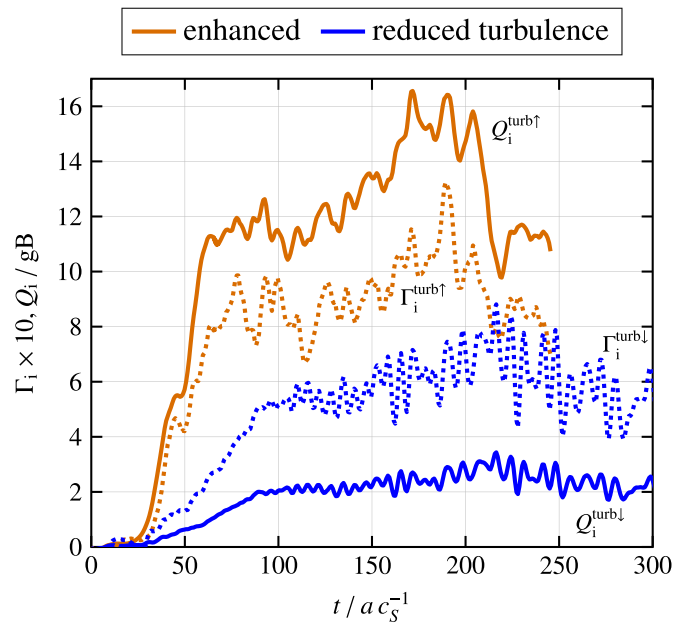


Figure 4. Ion heat flux Q_i (solid) and particle flux Γ_i (dotted and up-scaled by a factor of 10) from non-linear simulations as a function of the time for the enhanced (orange, 20 180 919.049) and reduced (blue, 20 180 919.007) turbulence scenario.

profile, which is a characteristic feature of W7-X [16, 17, 40]. At the same time, the reduction of the main ions particle flux seems less significant, but it is important to note that those fluxes are produced with very different normalized density gradients, $a/L_{n_e}^{\text{turb} \uparrow} = 0.6$ and $a/L_{n_e}^{\text{turb} \downarrow} = 2.1$ respectively. This results into a diffusivity 3.5 times higher in the turbulence enhanced case than in the reduced turbulence case (assuming pure diffusion for the fluxes). It should be emphasized that this

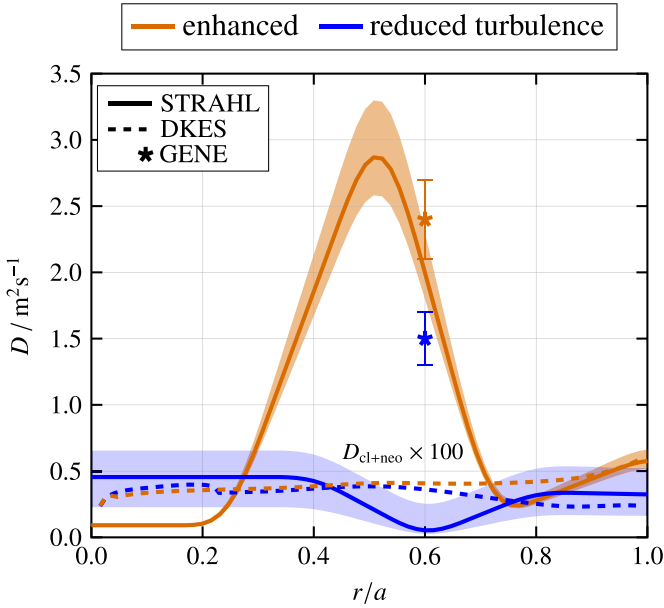


Figure 5. Radial profiles of the anomalous and collisional (classical and neoclassical, dashed lines, scaled up by a factor of 100) diffusion coefficient for Fe^{25+} as a function of the plasma radius for the enhanced (orange, 20 180 919.049) and reduced (blue, 20 180 919.007) turbulence scenario calculated with the 1D transport code STRAHL (solid lines and shaded areas) and dedicated points from non-linear GENE calculations (*).

is a reduction of the same order of magnitude for the particle and temperature transport coefficients D_i and χ_i .

We also compare the density fluctuation level measured by the phase contrast imaging (PCI) diagnostic [41, 42] and estimated by GENE. PCI measurements are located at a specific position of the GENE flux-tube considered in our study (most unstable flux-tube: located at the bean shaped W7-X cross-section). We compare the fluctuations produced only in that particular toroidal position (cross-section), as previously characterized and analyzed [38]. One should keep in mind that the flux-tube considered is not exactly the flux-tube that goes through the poloidal location of the PCI line of sight, but both flux-tubes exhibit similar electron density fluctuations and match well with the line integrated PCI signal [38]. The ratio of the fluctuation level between the two scenarios averaged in time $\langle \tilde{n}_e \rangle_t^{\text{turb}\uparrow} / \langle \tilde{n}_e \rangle_t^{\text{turb}\downarrow}$ match well. These amounts for PCI $\langle \tilde{n}_e \rangle_t^{\text{turb}\uparrow} / \langle \tilde{n}_e \rangle_t^{\text{turb}\downarrow} = 2.2$ and for GENE $\langle \tilde{n}_e \rangle_t^{\text{turb}\uparrow} / \langle \tilde{n}_e \rangle_t^{\text{turb}\downarrow} = 2.0$. This figure of merit evaluates the variation of the fluctuation magnitude excluding any unit or method dependence. It should be noted that the PCI value originates from line-integrated measurements along a radial line of sight, while the GENE value corresponds to radially local fluctuations. The radial localization of the turbulence, figure 5, makes the comparison valid.

In our turbulent transport modelling for Fe impurities, the reduced turbulence scenario is purely diffusive and equation (1) is simplified to $\Gamma_{\text{total}}^{(Z)\text{turb}\downarrow} \approx \Gamma_D^{(Z)\text{turb}\downarrow} = -D_Z^{\text{turb}\downarrow} \nabla n_Z$ with a diffusivity $D_Z^{\text{turb}\downarrow}$ responsible for the total flux. However, the enhanced turbulence scenario has two

important contributions to the total flux in equation (1): diffusion ($\Gamma_D^{(Z)\text{turb}\uparrow}$) and pinch (thermo-diffusion and curvature $\Gamma_V^{(Z)\text{turb}\uparrow}$). The latter with a significant velocity $|v| \approx 1 \text{ ms}^{-1}$. These fluxes have opposite directions, $\Gamma_D^{(Z)\text{turb}\uparrow} > 0$ and $\Gamma_V^{(Z)\text{turb}\uparrow} < 0$, which translates in a total particle flux smaller than the diffusive flux $|\Gamma_{\text{total}}^{(Z)\text{turb}\uparrow}| < |\Gamma_D^{(Z)\text{turb}\uparrow}|$. To calculate the diffusivity, first, we must estimate $\Gamma_D^{(Z)\text{turb}\uparrow}$ using the total flux $\Gamma_{\text{total}}^{(Z)\text{turb}\uparrow}$ produced by the simulation with all the gradients included and the pinch flux $\Gamma_V^{(Z)\text{turb}\uparrow}$ produced by the simulation with no density gradient included. The $\Gamma_D^{(Z)\text{turb}\uparrow}$ is defined as: $\Gamma_D^{(Z)\text{turb}\uparrow} = \Gamma_{\text{total}}^{(Z)\text{turb}\uparrow} - \Gamma_V^{(Z)\text{turb}\uparrow} = -D_Z \nabla n_Z$. With all these considerations, the transport coefficient for the enhanced turbulence scenario is $D_Z^{\text{turb}\uparrow} = 2.4 \pm 0.3 \text{ m}^2 \text{ s}^{-1}$ and for the reduced turbulence scenario is $D_Z^{\text{turb}\downarrow} = 1.5 \pm 0.2 \text{ m}^2 \text{ s}^{-1}$, see figure 5. As expected, the enhanced turbulence scenario has a stronger diffusivity than the reduced turbulence scenario and produces a diffusive flux of the same order with a smaller gradient.

4. Discussion and conclusions

Comparing the GENE results for diffusivity with the STRAHL estimates of anomalous D_Z , see figure 5, we find good agreement for the enhanced turbulence scenario. These results are robust and consistent, finding similar results for other discharges in a previous analysis [43]. In the reduced turbulence scenario, we capture a significant suppression of the turbulent transport for the main ions due to the density peaking, which translates to a substantial reduction of the diffusive coefficient for the impurities. Trends are clear and values are on the same order of magnitude (in contrast with the neoclassical estimations, two orders of magnitude smaller), but the matching between the GENE and STRAHL estimations is not as good as in the previous scenario. There are two potential contributions not accounted for in the GENE calculation that could complement the total transport reduction observed by STRAHL: collisions and the radial electric field E_r . These corrections to our GENE modelling were not initially included because massively increase the number of simulations and the computational demands, exceeding, by far, our computational possibilities. Regarding collisions, the density peaking should increase the number of collisions which reduces the TEM-instability by de-trapping the electrons of the bad curvature regions [44]. However, in the turbulence enhanced scenario, ITG is the dominant instability, which is almost immune to the effects of collisions [16], and the possible contribution is small. For the reduced turbulence scenario, figure 3 shows important ITG and TEM (produced by the density gradient) instabilities. However, TEM turbulence is significantly suppressed during the non-linear simulations due to the quasi-isodynamic property of W7-X [10, 17]. ITG instability also dominates this scenario, and collisions will not have an important impact on our results. The radial electric field has previously shown an important role suppressing




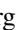





turbulent transport in W7-AS [45]. In stellarator geometry, the E_r induces a poloidal rotation on the magnetic surface, moving the fluctuations out of the bad curvature regions and reducing the turbulent heat losses. In our discharge, E_r (see figure 2(c)) is negatively increased during the reduced turbulence scenario. In particular, for W7-X we have a recent estimation of this effect (excluding the radial shear that would have a small impact because E_r is maximum in the position of interest) with very similar conditions of density peaking during a pellet discharge [17]: same magnetic configuration, same E_r , similar gradients and similar plasma parameters. In [17] the reduction on the main ions turbulence due to the density peaking (kinetic species, flux-tube simulations) is compared with the reduction of the radial electric field (adiabatic electrons, flux-surface simulations). The study concludes that both reductions are relevant and in a similar order of magnitude, however, the reduction due to the density gradient seems to be higher at present conditions. According to these results, we can expect a reduction of the same order of magnitude as that produced by the density-peak mechanism, which agrees well with our gap between the GENE and STRAHL calculations.

We modelled the turbulent impurity transport of W7-X, performing a first direct comparison between turbulent impurity transport coefficients calculated with GENE and those experimentally obtained from STRAHL for a specific W7-X discharge. In particular, two scenarios differing in turbulence level were investigated. In contrast to the neoclassical estimations that were, by far, insufficient, in both scenarios the numerical estimates of turbulence can account for the experimental impurity transport observed in the device. In particular, the enhanced turbulent scenario has a good agreement in order of magnitude and values for the transport coefficients. In this scenario, the transport is dominated by turbulence and the injected Fe-impurities are kicked out quickly, which results into a low confinement and short transport times. During the reduced turbulence scenario, the transport coeff. estimated with our modeling is one order of magnitude higher than the experimentally observed. In this scenario, the impact of turbulence is significantly suppressed for main ions and impurities. As a result, the confinement of Fe impurities is higher and the transport times longer. The enhanced turbulence scenario is well described by our gyro-kinetic model which produces similar estimations for the transport coefficients. The characteristic reduction of turbulence due to the density peaking observed during the reduced turbulence scenario is also well captured by our model, however, the diffusive transport coefficient is overestimated, likely due to the absence of the E_r effects previously shown to be effective in reducing turbulence. Next computational efforts together with dedicated W7-X experiments during the W7-X OP2 campaign will be devoted to obtain a full radial profile characterization of turbulent transport and to capture the complete effect of the E_r . These modelling results represent the definitive evidence of a dominant turbulent contribution to the transport of impurities for ECRH plasma conditions in W7-X, which had previously been highlighted and discussed using indirect methods.

Acknowledgments

This work has been carried out within the framework of the EUROfusion Consortium, funded by the European Union via the Euratom Research and Training Programme (Grant Agreement No 101052200 - EUROfusion). Views and opinions expressed are however those of the author(s) only and do not necessarily reflect those of the European Union or the European Commission. Neither the European Union nor the European Commission can be held responsible for them. The study has also been supported by Consejería de Transformación Económica, Industria, Conocimiento y Universidades de la Junta de Andalucía (reference POSTDOC_21_00631). GENE simulations have been conducted on the Marconi supercomputer (Italy), on the Cobra supercomputer (Garching, Germany) and on the Uranus supercomputer (Universidad Carlos III de Madrid, Spain) funded jointly by EU-FEDER funds and by the Spanish Government via the National Projects Nos. UNC313-4E2361, ENE2009-12213-C03-03, ENE2012-33219, ENE2012-31753 and ENE2015-68265-P. Work of US participants supported by the US DOE Grant DE-SC0014229.

ORCID iDs

J.A. Alcusón  <https://orcid.org/0000-0001-5492-7432>
 Th. Wegner  <https://orcid.org/0000-0003-0136-0406>
 A. Dinklage  <https://orcid.org/0000-0002-5815-8463>
 A. Langenberg  <https://orcid.org/0000-0002-2107-5488>
 J.-P. Böhner  <https://orcid.org/0000-0002-5828-2747>
 B. Buttenschön  <https://orcid.org/0000-0002-9830-9641>
 J.M. García-Regaña  <https://orcid.org/0000-0001-7632-3357>
 P. Xanthopoulos  <https://orcid.org/0000-0003-3545-4822>
 A. Zocco  <https://orcid.org/0000-0003-2617-3658>

References

- [1] Connor J.W. 1973 *Plasma Phys.* **15** 765
- [2] Igitkhanov Y., Polunovsky E. and Beidler C.D. 2006 *Fusion Sci. Technol.* **50** 268
- [3] Velasco J. et al (The LHD Experimental Team and The TJ-II Team) 2016 *Nucl. Fusion* **57** 016016
- [4] Helander P., Newton S.L., Mollén A. and Smith H.M. 2017 *Phys. Rev. Lett.* **118** 155002
- [5] Beidler C.D. et al 2021 *Nature* **596** 221
- [6] Klingner T. et al (The W7-X Team) 2019 *Nucl. Fusion* **59** 112004
- [7] Geiger B. et al (The W7-X Team) 2019 *Nucl. Fusion* **59** 046009
- [8] Wegner T. et al 2020 *Nucl. Fusion* **60** 124004
- [9] Langenberg A. et al (The W7-X Team) 2020 *Phys. Plasmas* **27** 052510
- [10] Proll J.H.E., Helander P., Connor J.W. and Plunk G.G. 2012 *Phys. Rev. Lett.* **108** 245002
- [11] Proll J.H.E., Xanthopoulos P. and Helander P. 2013 *Phys. Plasmas* **20** 122506
- [12] Horton W., Choi D. and Tang W.M. 1981 *Phys. Fluids* **24** 1077
- [13] Romanelli F. 1989 *Phys. Fluids B* **1** 1018
- [14] Xu X.Q. and Rosenbluth M.N. 1991 *Phys. Fluids B* **3** 627

- [15] Baldzuhn J. *et al* 2020 *Plasma Phys. Control. Fusion* **62** 055012
- [16] Alcusón J.A., Xanthopoulos P., Plunk G.G., Helander P., Wilms F., Turkin Y., von Stechow A. and Grulke O. 2020 *Plasma Phys. Control. Fusion* **62** 035005
- [17] Xanthopoulos P. *et al* (The W7-X Team) 2020 *Phys. Rev. Lett.* **125** 075001
- [18] Helander P. and Zocco A. 2018 *Plasma Phys. Control. Fusion* **60** 084006
- [19] García-Regaña J.M. *et al* 2021 *J. Plasma Phys.* **87** 855870103
- [20] García-Regaña J.M., Barnes M., Calvo I., González-Jerez A., Thienpondt H., Sánchez E., Parra F.I. and St.-Onge D.A. 2021 *Nucl. Fusion* **61** 116019
- [21] Thienpondt H. *et al* (The W7-X Team) 2022 Turbulence prevents core particle depletion in stellarators (arXiv:2209.04194)
- [22] Andreeva T. 2002 *Vacuum Magnetic Configurations of Wendelstein 7-X Type IPP III/270* Max-Planck-Institut für Plasmaphysik (available at: <https://hdl.handle.net/11858/00-001M-0000-0027-450D-A>)
- [23] Wegner T. *et al* (The W7-X Team) 2018 *Rev. Sci. Instrum.* **89** 073505
- [24] Wegner T. *et al* 2020 *Rev. Sci. Instrum.* **91** 083503
- [25] Bertschinger G., Biel W., Jaegers H. and Marchuk O. 2004 *Rev. Sci. Instrum.* **75** 3727
- [26] Langenberg A. *et al* (The W7-X Team) 2017 *Nucl. Fusion* **57** 086013
- [27] Hirshman S., van Rij W. and Merkel P. 1986a *Comput. Phys. Commun.* **43** 143
- [28] Pasch E., Beurskens M.N.A., Bozhenkov S.A., Fuchert G., Knauer J. and Wolf R.C. 2016 *Rev. Sci. Instrum.* **87** 11E729
- [29] Hirshman S.P., Shaing K.C., van Rij W.I., Beasley C.O. and Crume E.C. 1986 *Phys. Fluids* **29** 2951
- [30] Maassberg H. *et al* 1993 *Plasma Phys. Control. Fusion* **35** B319
- [31] Biel W., Bertschinger G., Burhenn R., König R. and Jourdain E. 2004 *Rev. Sci. Instrum.* **75** 3268
- [32] Behringer K. 1987 Description of the impurity transport code "Strahl" (JET-R(87) 08 (JET Joint Undertaking, Abingdon) (available at: <http://aei.pitt.edu/57921/1/JET.J.U.1987.pdf>)
- [33] Landreman M., Smith H.M., Mollén A. and Helander P. 2014 *Phys. Plasmas* **21** 042503
- [34] LaBombard B. 2001 Kn1d: A 1D space, 2D velocity, kinetic transport algorithm for atomic and molecular hydrogen in an ionizing plasma *Type Psfc/RR-01-3* (Institution Plasma Science and Fusion Center, Massachusetts Institute of Technology)
- [35] Jenko F., Dorland W., Kotschenreuther M. and Rogers B.N. 2000 *Phys. Plasmas* **7** 1904
- [36] Xanthopoulos P., Mynick H.E., Helander P., Turkin Y., Plunk G.G., Jenko F., Görler T., Told D., Bird T. and Proll J.H.E. 2014 *Phys. Rev. Lett.* **113** 155001
- [37] Navarro A.B. *et al* 2020 *Plasma Phys. Control. Fusion* **62** 105005
- [38] Böhner J.-P. *et al* 2021 *J. Plasma Phys.* **87** 905870314
- [39] Plunk G.G. *et al* (The W7-X Team) 2019 *Phys. Rev. Lett.* **122** 035002
- [40] Thienpondt H., na J.M.G.-R., Calvo I., González-Jerez A., Barnes M., Parra F.I. and Davies R. 2022 *Int. Stellarator and Heliotron Workshop (Warsaw)*
- [41] Edlund E.M., Porkolab M., Huang Z., Grulke O., Böttger L.-G., von Sehren C. and von Stechow A. 2018 *Rev. Sci. Instrum.* **89** 10E105
- [42] Huang Z., Edlund E., Porkolab M., Böhner J.-P., Böttger L.-G., v. Sehren C., von Stechow A. and Grulke O. 2021 *J. Instrum.* **16** P01014
- [43] Klinger T. 2020 *the Stellarator Dynamics, and T. Division IPP programme days 2020* (IPP)
- [44] Vernay T., Brunner S., Villard L., McMillan B., Jolliet S., Bottino A., Goerler T. and Jenko F. 2013 *Plasma Phys. Control. Fusion* **55** 074016
- [45] Wagner F. *et al* 2005 *Phys. Plasmas* **12** 072509